Journal of Imaging Science and Technology® 52(6): 060506–060506-8, 2008.

Predictive Design of Paper Microstructure for Xerographic Printing

Tao Wu and Nikolas Provatas
Department of Materials Science and Engineering, Brockhouse Institute for Materials Research, McMaster University, Hamilton, Ontario L8S 4L7, Canada
E-mail: provata@mcmaster.ca

Chaohui Tong
Departments of Materials Science and Engineering, McMaster University and Max-Planck Institute for Polymer Research, Mainz, Germany

Abstract. *The authors present a new approach for modeling toner transfer in xerographic printing. Our formalism combines a new three-dimensional (3D) stochastic fiber network model of paper, a 3D model of electrostatic, and contact adhesion forces acting on toner particles in xerographic printing. Our modeling platform allows the authors to study the relative importance of paper surface and mass density variations in establishing the electrostatic and contact adhesion forces crucial in controlling toner transfer efficiency during xerography. Simulations of xerographic printing are used to show that state of compression of the paper surface in the print nip is critical in controlling the distribution of toner onto paper. This is quantified by showing how the paper surface controls the distribution of both the electrostatic and contact adhesion forces that draw toner to paper. In contrast, paper formation, a traditional index of paper quality in the paper industry, is found to play a negligible role as a predictive measure of print uniformity in xerographic printing. Our simulation results are validated against new xerographic printing experiments of black toner onto laboratory handsheets. © 2008 Society for Imaging Science and Technology.*
[DOI: 10.2352/J.ImagingSci.Technol.(2008)52:6(060506)]

INTRODUCTION

Xerography has undergone very rapid development in recent years, with focus shifting from traditional black and white copying and printing to full-color printing. With the use of smaller toner particles for higher image quality, understanding the mechanisms controlling the uniformity of toner transfer onto an inherently nonuniform printing substrate such as paper is arguably one of the most important aspects in the design of improved commercial digital printing papers.

Predictive design of digital printing paper has traditionally been very difficult due to the complex nature of paper microstructure. From the first one dimensional model of toner transfer process by Yang and Hartmann,[1] most research on electrophotographic printing (of which xerography is an example) has assumed print substrates are dielectrically and structurally homogenous.[2–5] In reality, paper is a highly heterogeneous medium.[6–11] The most common stochastic measures of paper structure include mass density, surface roughness, filler distribution, and moisture. These properties all influence the local dielectric properties of paper, thus affecting the uniformity of the electrostatic forces used to help transfer toner to paper, a major factor controlling print uniformity.

Recent research has shown that paper surface variation is the most important measure of paper heterogeneity controlling the spatial variations of the electrostatic field responsible for toner transfer uniformity in xerography. Studies have involved experimental analysis of handsheets and commercial printing paper,[9] mathematical analysis of electrostatic field response to surface and bulk variations,[12] and the use of realistic simulated three-dimensional (3D) fiber webs to examine paper heterogeneity on electrostatic transfer forces.[11–13] All these studies further suggest that formation is negligible in establishing the electrostatic bias field controlling toner transfer uniformity.

Many previous studies such as those in by Tong et al.[11] were done under the assumption that the paper suffers no deformation in the z direction during its passage through the print nip. In this limit toner transfer is essentially effectuated by the competition between the electrostatic field, established entirely by the original paper structure, and toner adhesion forces.[1] It is reasonable to expect that papers passing through a print nip will experience a certain degree of surface deformation, which will in turn affect the electrostatic and contact adhesion landscape controlling toner transfer onto the paper. This hypothesis is also supported by other recent experimental works.[14–16]

This article examines the role that nip-deformed paper structure plays in shaping the electrostatic transfer forces and adhesion forces that are responsible for transferring toner to paper in xerographic printing. The next section briefly summarizes a new simulation platform for computing toner transfer forces corresponding to different 3D paper structures under different states of paper-nip deformations. By accounting for both electrostatic and adhesion forces acting on toner particles, our simulation platform allows toner transfer distributions to be predicted. We then describe new

Received Feb. 28, 2008; accepted for publication Sep. 5, 2008; published online Dec. 10, 2008.
1062-3701/2008/52(6)/060506/8/$20.00.

experiments which measure the distribution of black toner onto laboratory handsheets under conditions of commercial xerography, and compare simulations from our modeling platform to our experimental toner distributions. Results are used to elucidate the roles that the paper surface, mass density, and surface deformation have on toner transfer uniformity. The Conclusions and Discussion section discusses the significance of our results in the context of commercial xerographic image quality.

MODELING TONER TRANSFER ONTO PAPER

Modeling Paper Structure and Its z-Direction Compression

Our modeling platform simulates paper webs using a 3D random fiber deposition model introduced by Provatas and Uesaka.[10] In this model, fibers are sequentially deposited, one at a time, onto a fiber web. Individual fiber dimensions are drawn from a prescribed statistical distribution. In this work a Poisson distribution is used, as this has been found to give good agreement with experimental fiber length distributions.

Fibers are also endowed with a degree of flexibility and collapsibility in the z direction. Both these attributes are meant to emulate the packing of a fiber network under a certain degree of draining pressure during forming. Fiber collapse and bending can be formally linked to fiber-mechanical properties and a mean-field drainage pressure parameter.[10] It is usually simpler, however, to treat the degree of collapse and flexibility as phenomenological and to use a value that reproduces experimental surface and bulk statistics of paper samples.

Simulated fiber centers are distributed using a flocculation parameter developed in Provatas and Uesaka,[11] which generalizes a two-dimensional (2D) deposition process originally developed by Provatas et al. [17] This allows us to generate paper webs with formation ranging from ultrauniform to highly flocculated. The nature of this parameter is presently phenomenological, but can quite readily be calibrated to generate highly realistic virtual paper substrates.

After a simulated paper web is deposited, its surface (and interior bulk) can also be compressed from the top in the z direction (direction of toner transfer). This feature is important to be able to capture deformation of paper in the print nip. The paper compression phase of the model is summarized as follows.

The 3D paper web is decomposed into in-plane (i.e., x, y) zones, each of which is assumed to hold a spring that deforms in the z direction. The tangent modulus of each spring depends on the fiber mass distributed within each spring's zone. Zone dimensions are set large enough so that springs can be assumed to be decoupled in the x-y plane. The linear dimension of each zone, denoted ξ, typically scales with the thickness of the paper (i.e., $\sim 10^2$ μm) and is typically smaller than the feature size of many visible print mottle defects. The z-direction height of each such spring is the mean web thickness averaged over the zone of the spring. As each "paper spring" is deformed incrementally, the coordinates of all fiber segments passing through the spring's zone are displaced into the z direction with a strain equal to that of the spring.

The stress versus strain response of each in-plane paper spring shares many similarities to a cellular material under loading.[18] At present only a few studies of paper compression have been done[19,20] and the precise nature of how a section of paper deforms in the z direction remains unclear. In this work we will tentatively assume that each paper spring follows a form we have observed experimentally, given by

$$\sigma_s = \sum_{n=1}^{4} c_n \varepsilon_s^{4-n}, \tag{1}$$

where σ_s and ε_s are the stress and strain in each spring, while the coefficients c_n have been derived from experiments on paper deformation using micro-indenters of varying diameters. In particular, $c_1 = 4 \times 10^7$, $c_2 = -3 \times 10^7$, $c_3 = 9 \times 10^6$, $c_4 = -299{,}683$; the units are Pa, $\mathrm{N/m^2}$. The full details will be presented in a separate study.[21]

Algorithmically, the theoretical formalism described above is implemented on springs of lateral dimensions 5×5 $\mu\mathrm{m}^2$, which are much smaller than the decoupling zone ξ. This still assures that the deformation of a simulated paper surface and bulk will be realistic on length scales larger than ξ, while it will only be qualitative on scales smaller than ξ. We note since in this investigation the precise nature of how simulated paper structure is generated is secondary to diagnosing how paper structure affects electrostatic transfer forces in the toner layer, the precise details of the paper structure model will not be discussed further here. The interested reader is referred to Ref. 10.

Figure 1(a) shows a typical simulated paper surface. The simulation corresponds to a laboratory handsheet of basis weight 36 $\mathrm{g/m^2}$ and average thickness 80 μm. Figure 1(b) shows the simulated handsheet after compressive loading of an infinitely stiff flat plate that compresses the paper by a strain of 0.083 of its maximum asperity height. Figure 1(c) compares the two-point correlation function of the surface variation of simulated handsheets to that of laboratory handsheets (described below). Figure 1(d) is the corresponding comparison for the mass distribution. The two-point correlation function characterizes the importance of a given length scale of variation in paper formation and surface topography.[11] Table I summarizes the properties of the simulated and experimental papers used in this study.

Modeling Electrostatic Transfer Forces on Toner Particles

The calculation of electrostatic toner transfer forces in the presence of an arbitrary dielectric distribution is obtained by solving the Poisson equations with a spatially non-uniform dielectric field, i.e.,

$$\vec{\nabla} \cdot (\varepsilon(\vec{x}) \vec{\nabla} \phi(\vec{x})) = -\rho(\vec{x}). \tag{2}$$

In Eq. (2) ϕ is the electrostatic potential, $\rho(\vec{x})$ is the free charge density in the region, such as paper surface charge or

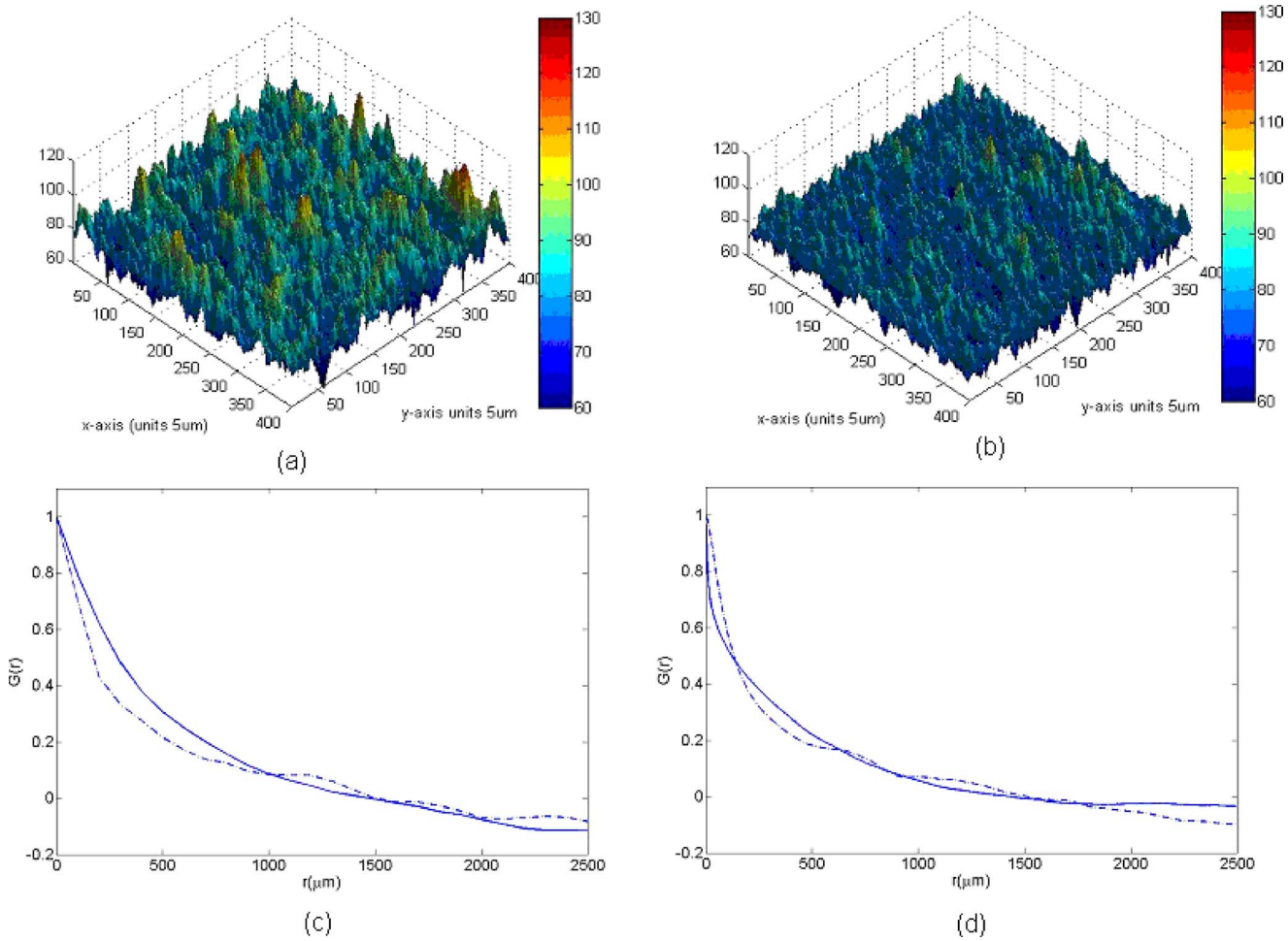

Figure 1. Simulated paper surfaces before (a) and after (b) compression. The axes are scaled in units of 5 μm. Paper basis weight is 36 g/m^2 and average paper caliper before compression is 80 μm. The paper is compressed to a mean strain of 0.083. (c) Plots of the two-point mass-mass correlation function for paper formation for simulated virtual (solid line) and experimental (dash-dot line) handsheet paper samples. (d) Plots of the two-point height-height correlation function for paper roughness simulated (solid line) and experimental (dash-dot line) handsheet paper samples.

Table I. Properties for simulation paper and experimental samples.

Properties	Samples	Simulation
Mean Mass	0.922 mg (5% water)	0.876
Mean Thickness	80 μm	79.49
Covariance of thickness	1.697	1.698
Covariance of formation ($\times 10^{-3}$ mg m^{-1})	1.219	1.266

toner charge, and $\varepsilon(\vec{x})$ is the local dielectric constant. In this work, the dielectric function within the volume of the paper is assigned from a discrete map of a 3D paper web generated from the random fiber network model described above, which can simulate up to three types materials; e.g., two types of fiber and filler. In the present study only laboratory handsheets comprising fibers and air will be considered. Commercial papers will be considered in a future study. The dielectric function also describes the toner layer, which in this work we assume to be a uniform layer 10 μm thick, carrying a uniform charge density of 32.43 C/m^3. The voltage used in the electrostatic toner transfer calculations is 1000 V.

Equation (2) is solved numerically using an efficient 3D multigrid algorithm[22] distributed across parallel processors. At the core of the multigrid is an iterative solver whose stencils are generated using a mesh of finite volumes. A finite volume formulation of the Poisson equation is typically better suited to handle abrupt changes of the dielectric function $\varepsilon(\vec{x})$. Precise details of the implementation of the multigrid code can also be found in Ref. 11 and will not be discussed further here.

Modeling Contact Forces and Toner Transfer Density onto Paper

In addition to the electrostatic forces acting on toners, adhesion forces must also be considered. In general, the adhesion force between the toner particles and photoreceptor is quite large. If the toner particle is to be transferred onto

paper solely by electrostatic bias, a large electrostatic transfer force has to be applied to offset the adhesion force between the toner particle and the photoreceptor, which would demand a very large electric field to be generated in the transfer nip. A high electric field can result in corona breakdown, or worse, sparking, which would greatly degrade the toner transfer process.

To obtain high transfer efficiency, paper typically needs to be compressed onto the photoreceptor to generate contact between the toner particles and paper fibers. The force between the toner particles and paper will offset the adhesion force between the toner particles and photoreceptor to some extent, making the toner particles easier to be transferred by the electrostatic bias field.

Our model incorporates paper-toner and toner-photoreceptor contact forces on toners, using adhesion forces that have been examined experimentally[23–27] and theoretically.[28–33] Figure 2 illustrates the various forces that our model can apply to an individual toner particle.

Algorithmically, if a toner particle resides over a paper valley where there is no direct contact between toner particle and the paper surface, a generic 500 nN toner-photoreceptor contact force is active in the positive z direction (toward the photoreceptor). Otherwise, a net adhesion force of 100 nN is applied to the toner in the positive z direction because the contact between toner and paper surface will offset most of the toner-photoreceptor force. This can be altered according to specific adhesion measurement data. The electrostatic bias field calculated from Eq. (2) is always in the negative direction (toward the paper). Toners with a net force (adhesion plus electrostatic bias) in the negative direction are marked for transfer onto the paper, otherwise they do not transfer. The final toner density distribution thus simulated is then coarse grained to the same resolution as our experiments, which in this work is 50 μm $\times$ 50 μm.

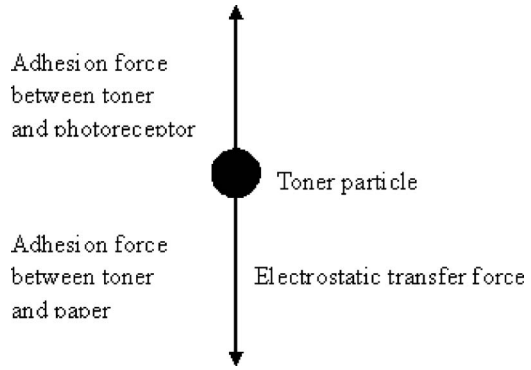

Figure 2. Illustration of various forces acting on a toner particle.

The multigrid code used to solve Eq. (2), the 3D paper structure model and the contact distribution mapping described above have been combined into an integrated simulation platform that can be used to simulate the efficiency of toner transferred onto different simulated paper structures and under varying degrees of surface deformation in the print nip. Figure 3 illustrates schematically the complete details of the modeling platform.

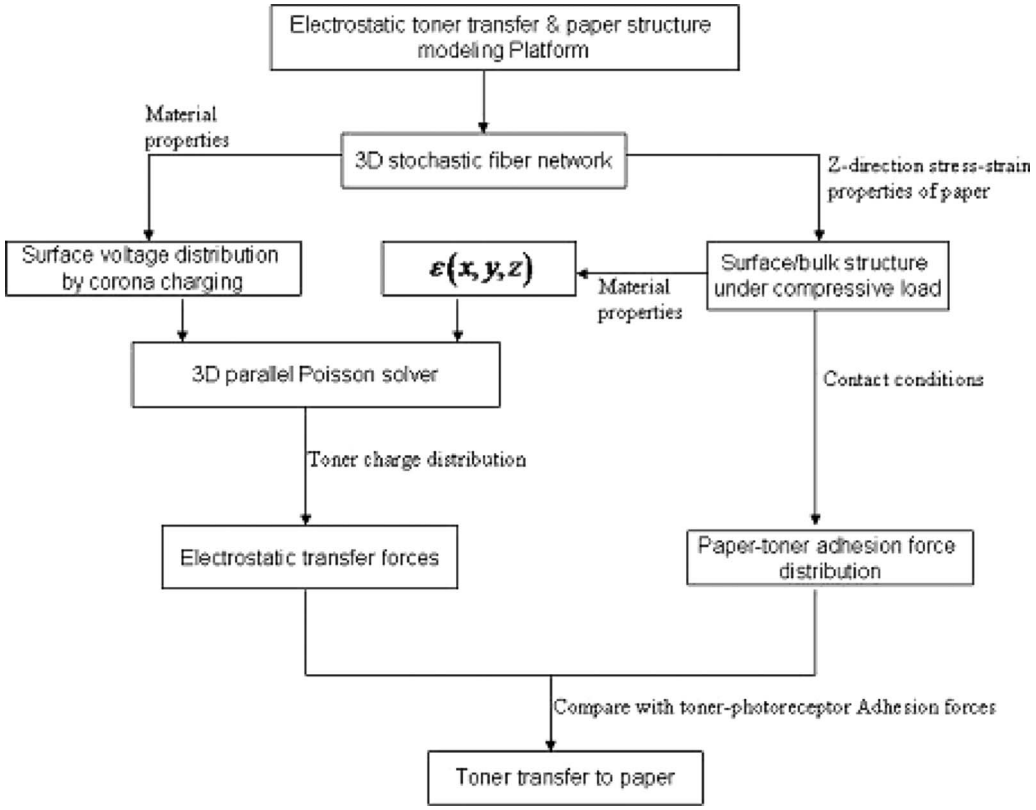

Figure 3. Schematic of the toner transfer and paper structure modeling platform.

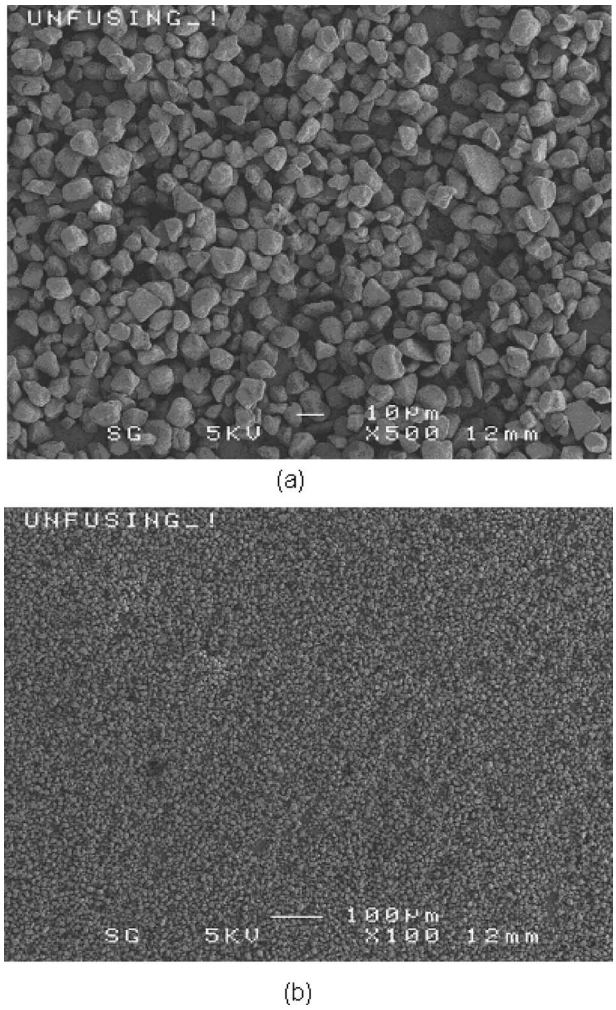

Figure 4. SEM image for toner particle distribution on a laboratory handsheet sample, under (a) 500× magnification and (b) 100× magnification

EXPERIMENTAL TONER TRANSFER DISTRIBUTIONS

Black toner was transferred using a Xerox DocumentColor 12 copier onto six 5×5 cm^2 areas of two laboratory handsheets samples of basis weight 36 g/m^2 which are prepared according to TAPPI standards. This copier was modified so that we could stop the printing process before the paper goes into the toner fusing stage, making it possible to study only the basic toner transfer process.

The toner particles used in this experiment are made from styrene and acrylic polymers, etc., and loaded to 10% by weight with carbon black. They are manufactured by the melt-mixing method. In general, colorants such as carbon black (or iron black) are first dispersed uniformly by blending into a melted thermoplastic resin, then, by extruding and cryogenic air-jet grinding, particles are obtained, which are classified into the desired particle size distribution. Finally, these are mixed with outer additives, such as fumed silica, to obtain the final product.[34–36] The average size of the toner particles is 10 μm and average toner charge is about 15 μC/g.

Figure 4 shows a scanning electron microscopy (SEM) image of toner particles distributed onto a printed area of a typical handsheet sample surface. The image suggests that toner particles are non-uniformly distributed in essentially one layer.

The printed 5×5 cm^2 subsections of our samples were scanned using a high-resolution scanner to obtain maps of reflected light intensity from the toner layer. This is a measure often used to quantify print mottle. Using the Image Processing Toolbox in MATLAB, the information from the reflected light image was converted to a digitized grayscale and stored as a 2D array for analysis. These data are indicative of the toner density distributions on the printed area. The size of the printed zones was dictated by the largest possible area of paper that we can simulate easily according to Eq. (2) given the memory of our present computing resources.

COMPARISON OF SIMULATIONS AND EXPERIMENT: PREDICTING TONER DENSITY DISTRIBUTION

This section examines the role that paper structure heterogeneity and paper-nip interactions have on toner transfer. It compares simulation results from our modeling platform with the toner transfer experiments described in the previous section, identifying attributes of paper structure and paper deformation which affect toner transfer.

Several simulated handsheet samples analogous to that in Fig. 1(a) were generated. Simulated handsheets had the same initial surface, thickness, and mass density statistics as the laboratory handsheets discussed in the Experimental Tuner Transfer Distributions section. These "virtual" handsheets were then compressed to several strain levels (0.05, 0.10, 0.20) of their maximum asperity height, yielding surfaces analogous to that shown in Fig. 1(b).

We computed the power spectra of mass density variation (formation) and surface variations of the resulting simulated handsheets. We also computed the power spectra of the predicted toner distribution onto these virtual handsheets. The power spectra of the experimental toner distributions described in the previous section were also obtained. Power spectra from the six printed experimental zones were averaged to reduce statistical fluctuations.

Power spectral analysis is a useful analysis tool in this context as it can help establish a correspondence in length scales between different signals that are noisy under visual inspection. Power spectral analysis uses Fourier transformation to transform signal from physical space to Fourier space, where signals are characterized in terms of their component frequencies. A frequency has a magnitude and a direction. All experimental and simulated power spectra reported here were circularly averaged so that they become only a function of $|k|$, the magnitude of the inverse wavelength, and not its orientation. This implies that the signals are isotropic, a reasonable assumption for handsheets. As an example, a paper surface height distribution can be decomposed into a Fourier series, comprising a superposition of sine waves of different frequencies, k. Smaller $|k|$ represent

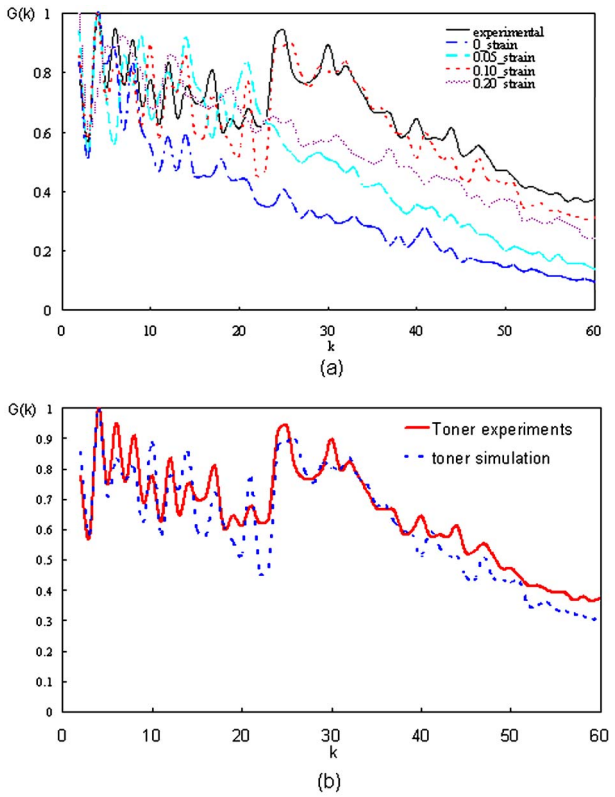

Figure 5. (a) Circularly averaged power spectra of: (i) toner density distribution obtained from simulation without compression (dash-dotted line); (ii) toner density distribution obtained from simulation under 0.05 strain (dash line); (iii) toner density distribution obtained from simulation under 0.10 strain (dotted line); (iv) toner density distribution obtained from simulation under 0.20 strain (shadow line); (v) toner density distribution obtained from experimentally printed zones (solid line). The x axis corresponds to wave number k. The wave number is in units of $2\pi/L$, with $L=512\times5$ μm. (b) Circularly averaged power spectra of: (i) toner density distribution obtained from simulation under 0.10 strain (dotted line) and (ii) toner density distribution obtained from experimentally printed zones (solid line). The x axis corresponds to wave number k. The wave number is in units of $2\pi/L$, with $L=512\times5$ μm

long wavelength sine waves and larger $|k|$ represent short wavelength sine waves. The combination of all sine waves with different k can reconstruct the paper surface. Power spectral analysis can also be used to similarly decompose the paper mass density distribution, electrostatic transfer force distribution and toner density distribution. Power spectra are normalized by their total area and averaged over several zones of the paper. Comparison of the resulting power spectra of two characteristics thus makes it possible to compare the relative importance of a given frequency (or feature scale) in the two measures.

Figure 5(a) compares the power spectra of the simulated toner distribution obtained with different strains of compression (in the print nip) applied to virtual handsheets. Also shown is the power spectrum of the toner distribution determined experimentally on the laboratory handsheets. Figure 5(b) isolates the case in Fig. 5(a) of 10% strain and the experimental curve. The simulation data suggest that at wavelengths larger than 500 μm ($k\equiv|k|<10$) paper compression does not play a large role in altering the toner transfer distribution, as all simulation data agree fairly well with

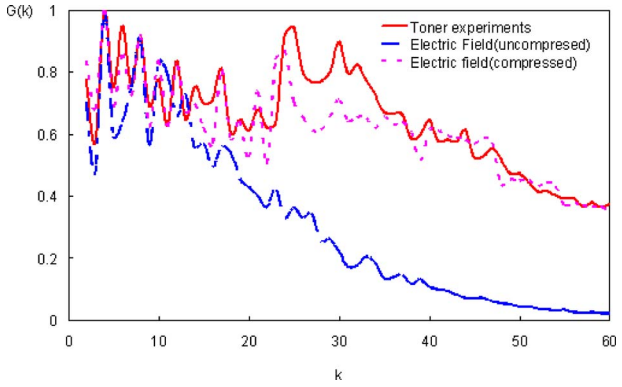

Figure 6. Circularly averaged power spectra of: (i) z component of electric field corresponding to uncompressed simulated paper webs (dash-dotted line); (ii) z component of electric field corresponding to compressed simulated paper webs (dotted line); and (iii) toner density distribution obtained from experimentally printed zones (solid line). The x axis corresponds to wave number k. The wave number is in units of $2\pi/L$, with $L=512\times5$ μm. Compression is at 0.1 strain.

the experimental data. For smaller wavelengths the power spectra of the simulated toner transfer distributions yield a good correspondence with experiments only if a certain degree of paper compression is accounted. In this case z-direction deformation of about 10% yields the best correspondence in the peak structure and intensity of simulated and experimental power spectra.

We note that the average pressure in the transfer nip of Xerox machine is on the order of 30 psi (1 psi= 6894.76 Pa). The resulting stress applied on the paper in transfer nip is thus about 206,842.8 Pa. From Eq. (1), the strain of the paper can be obtained, which is about 0.071,833 (7.18%). Hence, 10% strain for the paper in the transfer nip is a reasonable estimate of the z-direction paper strain in our Xerox engine experiments. It should also be pointed out that the stress due to the electrostatic bias field calculated from Eq. (2) (by application of Gauss's law) is about an order of magnitude smaller than the mechanical stress.

Figure 6 compares the power spectra of the electrostatic bias field simulated with and without 10% paper compression of the paper surface to that of the toner distribution determined experimentally. Good correspondence in the peak positions and the morphology of the power spectra of the toner distribution and the electrostatic field is obtained in the case of the compressed paper. This result is consistent with the results of Fig. 5(b), since the major transfer force acting on toner at long wavelengths is that from the electrostatic bias field.

Figure 7 compares the power spectra from simulated surface profiles corresponding to the 10% deformed paper and that from the undeformed paper with the power spectrum of the experimental toner density distribution. The figure shows that the compressed paper surface variations also correspond quite well with the toner density variations for almost the entire range of wavelengths. This result is consistent with the results of Figs. 5(b) and 6, since the surface of paper strongly modulates the electrostatic transfer field.[11] It is also consistent with the short wavelength results

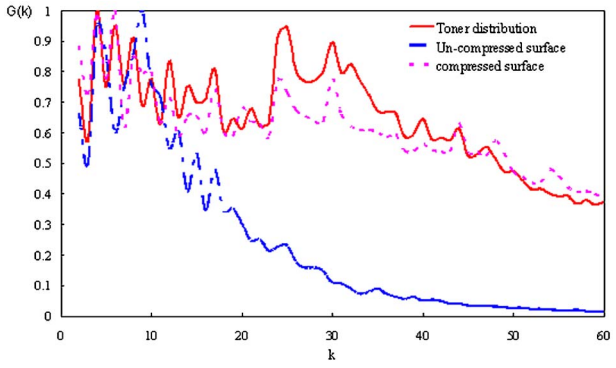

Figure 7. Circularly averaged power spectra of: (i) surface height of a simulated paper webs before compression (dash-dotted line); (ii) surface height of the simulated paper webs after compression (dotted line); and (iii) toner density distribution obtained from experimentally printed zones (solid line). The x axis corresponds to wave number k. The wave number is in units of $2\pi/L$, with $L=512\times5$ μm. Compression was at 0.1 strain.

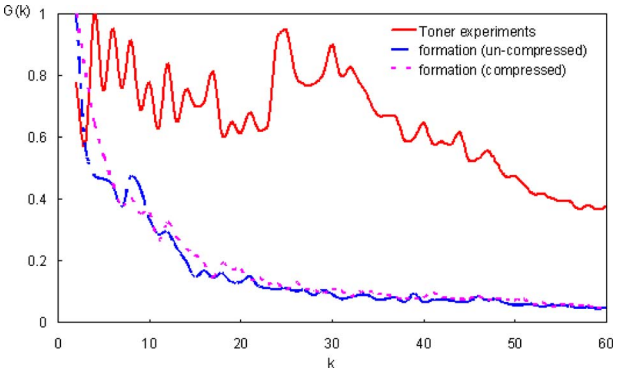

Figure 8. Circularly averaged power spectra of: (i) overall mass density from simulated paper webs before compression (dash-dotted line); (ii) overall mass density from simulated paper webs after compression (dotted line); and (iii) toner density distribution obtained from experimentally printed zones (solid line). The x axis corresponds to wave number k. The wave number is in units of $2\pi/L$, with $L=512\times5$ μm. Compression was at 0.1 strain.

of Fig. 5(b) if we note that the paper surface modulates the distribution of toner adhesion contact forces and these are expected to be an important transfer mechanism at small scales.

Figure 8 compares the power spectra of the mass variation (i.e., formation) in our simulated paper webs with the toner density distribution from our experiments. The data shows that there is very little correspondence between spatial variations in toner density and mass density at any wavelength. It is also clear that the formation is not correlated at all to the electrostatic field or surface profile. The latter result is explained by noting that surface profile variations occur closer to the toner layer than do bulk mass variations, thus exerting greater control on perturbations of the electrostatic field in the toner layer.[11,12]

Interpreting the above results in the context of Tong et al.[11] suggests that at long enough wavelengths the net toner transfer force is controlled by the electrostatic bias field, which is in turn predominately modulated by the compressed paper surface profile. On the other hand, as shown by Tong et al.,[11] the surface does not exercise much control over the electrostatic field at very small wavelengths. At these length scales, toner transfer density is likely controlled by toner-paper adhesion forces, which are also modulated by the (deformed) surface profile. These results suggest that the description of spatial variation of toner transfer requires detailed knowledge of the electrostatic toner transfer fields at long wavelengths and more precise information of toner adhesion forces with the photoreceptor and paper at small length scales. An important prediction of this work is that the effect of the paper surface on toner transfer must be assessed under of state of z compression.

CONCLUSIONS AND DISCUSSION

We have introduced a new modeling platform for computing how virtual paper structures and paper-nip interactions influence the toner transfer forces that arise during electrophotography. Comparison of our simulations with experiments indicates that above visible length scales (long wavelength scales, larger than 50 μm), toner density variations on printed handsheets are strongly correlated to those of the paper surface profile under a state of compression, which directly shapes the electrostatic field in the print nip. This suggests that the nip-deformed paper surface is critical in controlling the print quality results in toner transfer process.

On the small length scales, we note that the toner density distribution will no longer be correlated very well to the electrostatic transfer force distribution. In this regime, we believe that toner adhesion forces become more crucial. These as well, however, are modulated by the nip-deformed surface. As a result, the toner density distribution across all wavelengths is modulated by the combination of electrostatic transfer force and adhesion forces acting on length scales comparable to toner particle sizes.

Finally, our results independently confirm the conclusion of our previous work that bulk mass density (i.e., paper formation), which is often linked to good or bad print quality, is not a relevant index in electrophotographic print quality.

We believe that our results have significant ramifications on how digital printers and digital paper manufacturers view print substrates such as commercial printing paper. For instance, in manufacturing paper for digital printing, more attention should be paid to surface finish as opposed to the more traditional formation index. Also, it is well known that a coating layer is typically used to optimize print quality by improving the surface properties of the print substrate. We believe that a modeling platform like the one presented here can be useful in optimizing the mass and distribution of coating necessary to yield optimal transfer efficiency. Further work will be done in this area.

ACKNOWLEDGMENTS

The authors would like to thank the National Science and Engineering Research Council (NSERC) of Canada and Xerox Canada for financial support of this work. They are

also grateful to Gordon Sisler at the Xerox Research Centre, Canada (XRCC) for their toner transfer experiments, to Robert Pelton at McMaster University for providing them with experimental facilities, to Kari Dalnoki Verres at McMaster University for use of the microindentation apparatus, and to Steven Keller at the State University of New York, Syracuse, for betaradiography measurements. They also thank the Shared Hierarchical Academic Research Computing Network (SHARCNET: www.sharcnet.ca) for computing facilities.

REFERENCES

[1] C. C. Yang and G. C. Hartmann, "Electrostatic separation of a charged-particle layer between electrodes", IEEE Trans. Electron Devices **23**, 308–312 (1976).
[2] R. M. Schaffert, *Electrophotography* (Focal, New York, 1975), p. 30.
[3] L. B. Schein, *Electrophotography and Development Physics* (Springer, New York, 1988), p. 50.
[4] E. M. Williams, *The Physics and Technology of Xxerographic Process* (Wiley, New York, 1984), p. 100.
[5] D. M. Pai and B. E. Springett, "Physics of electrophotography", Rev. Mod. Phys. **65**, 163–211 (1993).
[6] K. J. Niskanen, *Paper Physics* (Fapet, Helsinki, 1998).
[7] J. Scharcanski and C. T. J. Dodson, "Neural network model for paper forming process", *IEEE Conference Record of Annual Pulp and Paper Industry Technical Conference* (IEEE, Piscataway, NJ, 1996) pp. 236–255.
[8] K. Niskanen and M. Alava, "Planar random networks with flexible fibers", Phys. Rev. Lett. **73**, 3475–3477 (1994).
[9] A. Cassidy, M. Grant, and N. Provatas, "Modeling dielectric heterogeneity in electrophotography", Modell. Simul. Mater. Sci. Eng. **12**, 97–107 (2004).
[10] N. Provatas and T. Uesaka, "Modeling paper structure and paper-press interactions", J. Pulp Pap. Sci. **29**, 332–340 (2003).
[11] C. Tong, T. Wu, and N. Provatas, "Modeling the role of paper microstructure in electrophotography", Modell. Simul. Mater. Sci. Eng. **14**, 1447–1464 (2006).
[12] J. Kallunki, M. Alava, and E. K. O. Hellen, "The electric field close to an undulating interface", J. Appl. Phys. **100**, 023528 (2006).
[13] T. Wu, C. Tong, and N. Provatas, "The role of paper-nip interactions on electrostatic toner transfer forces in xerographic printing", Int. J. Manuf. Tech. Manage. **14**, 52–65 (2008).
[14] D. S. Rimai and D. J. Quesnel, "Electrophotographic printing on textile and non-planar substrates", J. Imaging Sci. Technol. **48**, 10–14 (2004).
[15] G. Wright, T. N. Tombs, A. Chowdry, D. S. Weiss, and D. S. Rimai, "Toner transfer: Effects of size polydispersity", J. Imaging Sci. Technol. **49**, 531–538 (2005).
[16] D. S. Rimai, D. S. Weiss, and D. J. Quesnel, "Particle adhesion and removal in electrophotography", J. Adhes. Sci. Technol. **17**, 917–942 (2003).
[17] N. Provatas, M. Haataja, J. Asikainen, S. Majianiemi, M. Alava, and T. Alanissila, "Fiber deposition models in two and three spatial dimensions", Colloids Surf., A **165**, 209–229 (2000).
[18] L. J. Gibson and M. F. Ashby, *Cellular Solid: Structure and Properties* (Pergamon, Oxford, 1988).
[19] T. Yamauchi, "Compressibility of paper measured by using a rubber platen thickness gauge", Appita J. **43**, 222 (1989).
[20] S. Osaki and Y. Fujii, "On the z-direction compressive elasticity of paper", Tappi J. **32**, 476 (1978).
[21] T. Wu, B. Costa, and N. Provatas, "Measuring z-direction paper compression", preprint.
[22] W. L. Briggs, V. E. Henson, and S. F. McCormick, *A Multigrid Tutorial*, 2nd ed., (Sociey for Industrial and Applied Math, Philadelphia, 2000).
[23] D. A. Hays, "Electric field detachment of toner", Photograph. Sci. Eng. **22**, 232–235 (1978).
[24] C. J. Mastrangelo, "Effects of charge, size, and shape on toner photoconductor adhesion in elctrophotographic system", Photograph. Sci. Eng. **26**, 194–197 (1982).
[25] M. H. Lee and J. Ayala, "Adhesion of toner to photoconductor", J. Imaging Technol. **11**, 279–284 (1985).
[26] M. H. Lee and A. B. Jaffe, in *Particles on Surfaces 1: Detection, Adhesion, and Removal*, edited by K. L. Mittal (Plenum, New York, 1988), p. 169.
[27] L. B. Schein, W. S. Czarnecki, B. Christensen, T. Mu, and G. Galliford, "Experimental verification of the proximity theory of toner adhesion", J. Imaging Sci. Technol. **48**, 417–425 (2004).
[28] D. S. Rimai, D. J. Quesnel, L. DeMejo, and M. T. Regan, "Toner to photoconductor adhesion", J. Imaging Sci. Technol. **45**, 179–186 (2001).
[29] N. S. Goel and R. Spencer, in *Polymer Science Technology, Part B*, edited by L. H. Lee (Plenum, New York, 1975), p. 763.
[30] B. Gady, R. Reifenberger, D. M. Schaefer, R. C. Bowen, D. S. Rimai, L. DeMejo, and W. Vreeland, "Particle adhesion to elastomeric substrates and elastomeric subtrates with semi-rigid coatings", J. Adhes. **67**, 19–36 (1998).
[31] W. S. Czarnecki and L. B. Schein, "Electrostatic force acting on a spherically symmetric charge distribution in contact with a conductive plane", J. Electrost. **61**, 107–115 (2004).
[32] L. B. Schein and W. S. Czarnecki, "Electrostatic proximity force, toner adhesion, and atomic force microscopy of insulating particles", J. Electrost. **63**, 699–704 (2005).
[33] L. B. Schein and W. S. Czarnecki, "Proximity theory of toner adhesion", J. Imaging Sci. Technol. **48**, 412–416 (2004).
[34] B. Grushkin, "Processes for the preparation of toners", US Patent 5,145,762 (1992); L. DeMejo, J. M. McCabe, and J. C. Wilson, "Toner compositions containing a multi-purpose additive", US Patent 5,112,715 (1992).
[35] T. J. Fuller, A. C. VanLaeken, and W. M. Prest, "Toner polymers and processes thereof", US Patent 5,266,438 (1993).
[36] H. K. Mahabadi, E. E. Agur, G. R. Allison, M. S. Hawkins, S. Drappel, M. N. V. McDougall, B. Grushkin, T. R. Hoffend, and A. J. Barbetta, "Toners having cross-linked toner resins", US Patent 5,352,556 (1994).